

CMP: Cooperative Motion Prediction with Multi-Agent Communication

Zhuoyuan Wu^{1,*}, Yuping Wang^{2,*}, Hengbo Ma³, Zhaowei Li⁴, Hang Qiu^{5,†}, and Jiachen Li^{5,†}

Abstract—The confluence of the advancement of Autonomous Vehicles (AVs) and the maturity of Vehicle-to-Everything (V2X) communication has enabled the capability of cooperative connected and automated vehicles (CAVs). Building on top of cooperative perception, this paper explores the feasibility and effectiveness of cooperative motion prediction. Our method, CMP, takes LiDAR signals as input to enhance tracking and prediction capabilities. Unlike previous work that focuses separately on either cooperative perception or motion prediction, our framework, to the best of our knowledge, is the first to address the unified problem where CAVs share information in both perception and prediction modules. Incorporated into our design is the unique capability to tolerate realistic V2X bandwidth limitations and transmission delays, while dealing with bulky perception representations. We also propose a prediction aggregation module, which unifies the predictions obtained by different CAVs and generates the final prediction. Through extensive experiments and ablation studies, we demonstrate the effectiveness of our method in cooperative perception, tracking, and motion prediction tasks. In particular, CMP reduces the average prediction error by 17.2% with fewer missing detections compared with the no cooperation setting. Our work marks a significant step forward in the cooperative capabilities of CAVs, showcasing enhanced performance in complex scenarios.

I. INTRODUCTION

The current autonomous driving system is critically dependent on its onboard perception. Similar to human drivers, however, such dependency is vulnerable to situations with occlusions or impaired visibility. Leveraging multiple vantage points, cooperative perception [1]–[5] uses Vehicle-to-Everything (V2X) communications to share sensory information among connected and automated vehicles (CAVs) and infrastructure. This shared information varies in format, including raw data, processed features, or detected objects, along with relevant metadata (e.g., timestamps and poses). Fusing this information from multiple viewpoints to the perspective of a vehicle recipient, the *augmented* onboard perception can now “see” beyond their direct line of sight and through occlusions.

Current V2V research has largely been confined to either cooperative perception or motion prediction, with no comprehensive studies on their joint application. Beyond object detection, most works incorporate other tasks, such as prediction [3] and mapping [6] as auxiliary outputs. Wang *et al.* [3] proposes a V2V method for perception

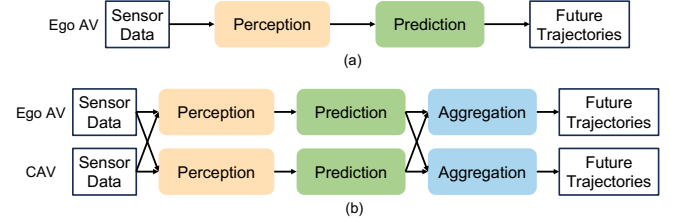


Fig. 1: A comparison between the traditional pipeline and the proposed multi-vehicle cooperative prediction pipeline. (a) The traditional pipeline conducts perception and prediction based on a single AV’s raw sensor data. (b) The proposed pipeline involves multiple cooperative CAVs, which share information to enhance both perception and prediction.

and prediction, which transmits intermediate representations of point cloud features. However, integrating perception and prediction, as illustrated in Fig. 1(b), to fully realize V2V cooperation remains unexplored. On motion prediction, initial efforts [7]–[9] use LSTM-based networks on simple datasets. Recent studies [10]–[12] adopt attention networks and graph convolutional networks to enhance motion prediction. However, these approaches rely on the ground-truth trajectory data, neglecting the uncertainties and inaccuracies propagated from upstream detection and tracking tasks. This reliance on ground truth data remains insufficient to address the real-world challenge of handling uncertain trajectories, underscoring the need for research that integrates perception and prediction in V2V cooperation.

To fill the gap between cooperative perception and motion prediction, we introduce a novel framework for cooperative motion prediction based on the raw sensor data. To the best of our knowledge, we are the first to develop a practical method that jointly solves the perception and prediction problem with CAV communications in both components. Our proposed framework is illustrated in Fig. 2. Each CAV computes its own bird-eye-view (BEV) feature representation from its LiDAR point cloud. The data is processed, compressed, and broadcast to other nearby CAVs. The receiver agents fuse the transmitted feature encoding. Upon obtaining historical perception data, the trajectories of the surrounding objects can be predicted by each CAV based on the backbone of MTR [10]. Then, the individually predicted trajectories from each CAV are broadcast again. As our model collects the predictions from surrounding CAVs, the predictions and intermediate features from perception are used to refine the motion predictions. Our method allows for realistic transmission delays between CAVs and bandwidth limitations while achieving satisfactory performance.

In this paper, our main contributions are as follows:

*Equal contribution

†Corresponding authors

¹Peking University, China. wuzhuoyuan@pku.edu.cn

²University of Michigan, Ann Arbor, MI, USA. ypw@umich.edu

³University of California, Berkeley, CA, USA. hengbo.ma@berkeley.edu

⁴University of Washington, WA, USA. lzw365@uw.edu

⁵University of California, Riverside, CA, USA. {hangqi, jiachen.li}@ucr.edu

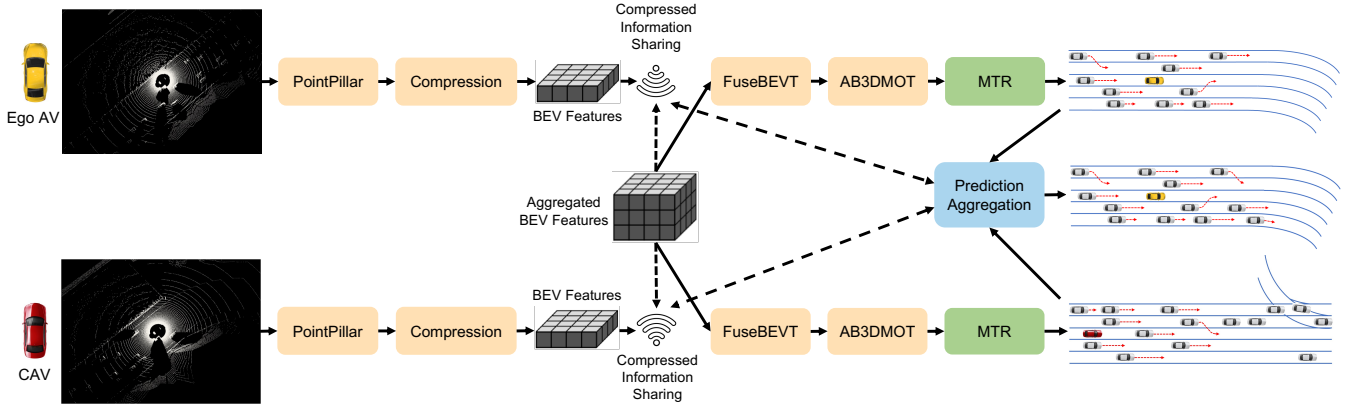


Fig. 2: An overall diagram of the proposed cooperative motion prediction pipeline.

- We propose a practical, latency-robust framework for cooperative motion prediction, which leverages the information shared by multiple CAVs to enhance perception and motion prediction performance.
- We analyze the bandwidth requirement for cooperative information sharing and design a lightweight representation for communication.
- We develop a transformer-based prediction aggregation module to take advantage of the predictions shared by other CAVs, which improves prediction accuracy.

II. RELATED WORK

A. Cooperative Perception

Cooperative perception allows CAVs to use advanced communication systems to share information to enlarge their fields of view. Previous works have developed early fusion techniques for cooperative object detection based on shared raw LiDAR or RGB camera data [2]. Using this strategy, however, requires high transmission bandwidth due to the preservation of complete sensor measurements. Another strategy, late fusion, allows vehicles to only share their final detections and rely on another model to fuse the detections generated by CAVs [13]. However, in real-life deployments, the performance of late fusion is capped by the loss of context information and individual detection accuracy.

To balance this trade-off, the middle-ground strategy of intermediate fusion [3], [5], [14], [15] has become more prevalent. In this strategy, CAVs employ encoder models to process the surrounding traffic information and map information to intermediate features, and then share these features with the surrounding vehicles. Upon receiving these features, CAVs fuse them with their own information and generate better perception results. For example, V2VNet [3] employed a Graph Neural Network to aggregate information from different viewpoints. AttFuse [4] deployed an attention mechanism to fuse the intermediate features. Qiao and Zulkernine [15] proposed a fusion model that adaptively chooses intermediate features for better integration. CoBEVT [5] and HM-ViT [16] have largely adopted vision transformer models to enhance camera input processing and feature integration and achieve promising results on the OPV2V dataset [4].

B. Motion Prediction

Motion prediction is another key research topic in autonomous driving. Mainstream research mostly focuses on a non-cooperative environment where a single AV predicts without communication [10], [17]–[28]. Recent methods [18], [24], [29] encode agent historical trajectories and map polylines into high-dimensional vectors and use graph neural networks to capture their relationships, which are followed by decoding layers to produce predictions. The most recent work introduced transformer structure into their models. MTR [10], MTR++ [11] use motion query pairs where each pair is in charge of one motion mode prediction, which is more efficient than goal-based strategies [30] and converges faster than direct regression strategies [21], [31].

III. PROBLEM FORMULATION

The goal of the cooperative prediction task is to infer the future trajectories of all the movable agents in the scene that can be detected by multiple collaborative CAVs with onboard sensors. In this work, we only use the LiDAR information for perception (i.e., object detection and tracking) to obtain the agents' trajectories. We denote the number of CAVs as N_{CAV} , the LiDAR point cloud of i -th CAV at time t as L_t^i , $i = 1, \dots, N_{CAV}$, and the local map information as M_t^i . Assume that there are N_t detected agents at time t , we denote their historical trajectories as $\mathbf{X}_{t-T_h+1:t}$ where T_h represents the history horizon. We aim to infer their multi-modal future trajectories $\hat{\mathbf{X}}_{t+1:t+T_f}$ based on the above information where T_f represents the prediction horizon.

IV. METHOD

A. Method Overview

Fig. 2 provides an overall diagram of our framework, which consists of three major components: cooperative perception, trajectory prediction, and prediction aggregation. The cooperative perception module takes in the raw sensor data obtained by CAVs and generates the observed agents' trajectories through object detection and multi-object tracking. Then, the trajectory prediction module takes in the historical observations and infers future trajectories from the perspective of each CAV. Finally, the prediction aggregation

module leverages the predictions from all CAVs and generates the final prediction hypotheses.

B. Cooperative Perception

The cooperative perception module aims to detect and track objects based on the 3D LiDAR point clouds obtained by multiple CAVs. We modify CoBEVT [5] to serve as the backbone of the cooperative object detection model followed by the AB3DMOT tracker [32] to obtain historical trajectories of agents.

Cooperative Object Detection. PointPillar [33] is employed to extract point cloud features for each CAV with a voxel resolution of (0.4, 0.4, 4) along x , y , and z axes. Before the cross-agent collaboration, each CAV i calculates a bird-eye-view (BEV) feature $\mathbf{F}^i \in \mathbb{R}^{H \times W \times C}$, where H , W , and C denote height, width, and channels, respectively.

Due to the real-world hardware constraints on the volume of the transmitted data for V2V applications, it is necessary to compress the BEV features before transmission to avoid large bandwidth-induced delays. As in [5], a convolutional auto-encoder is used for feature compression and decompression. Upon receipt of the broadcast messages containing intermediate BEV representations and the sender's pose, a differentiable spatial transformation operator Γ_ξ is used to align the features to the ego vehicle's coordinate, which is written as $\mathbf{H}^i = \Gamma_\xi(\mathbf{F}^i) \in \mathbb{R}^{H \times W \times C}$. Our method allows for up to a 100 ms latency during feature transmission by taking in the messages sent by other CAVs at the last frame. Since sensors refresh faster than 10 fps, frames taking longer than 100 ms to transmit (e.g. partially retransmitted or lost) will be dropped, and the latest frame will be used instead.

Then, FuseBEVT [5] is used to merge the BEV features received from various agents. More specifically, the ego vehicle first aggregates all the available features into a tensor $\mathbf{h} \in \mathbb{R}^{N_{\text{CAV}} \times H \times W \times C}$, which is then processed by the FuseBEVT module to obtain the fused feature $\mathbf{h}' \in \mathbb{R}^{H \times W \times C}$. Finally, two 3×3 convolutional layers are applied for classification and regression to obtain the 3D bounding boxes of objects.

CoBEVT outputs a collection of detections at time t denoted by $\mathbf{D}_t = \{\mathbf{D}_t^1, \dots, \mathbf{D}_t^{N_t}\}$, where N_t represents the total number of detections. Each detection \mathbf{D}_t^j is characterized by a tuple $(x, y, z, \theta, l, w, h, s)$, which encapsulates the 3D coordinates of the object's center (x, y, z) , the 3D dimensions of the object bounding box (l, w, h) , the orientation angle θ , and the confidence score s .

Multi-Object Tracking. The tracking module is employed to associate the detected 3D bounding boxes of objects into trajectory segments. We adopt AB3DMOT [32], an online multi-object tracking algorithm, which takes in the detections in the current frame and the associated trajectories in previous frames. Excluding the pre-trained cooperative object detection module, AB3DMOT requires no additional training and is simply applicable for inference.

More specifically, after obtaining the 3D bounding boxes from the cooperative object detection module, we apply a 3D Kalman filter to predict the state of the associated trajectories from previous frames to the current frame. Then,

a data association module is adopted to match the predicted trajectories from the Kalman filter and the detected bounding boxes in the current frame. The 3D Kalman filter updates the state of matched trajectories based on the matched detections. Throughout the tracking process, a birth and death memory creates trajectories for new objects and deletes trajectories for disappeared objects. More details of these operations can be found in [32]. The tracker outputs the historical trajectories of all the agents detected at time t , denoted as $\mathbf{X}_{t-T_h+1:t}$, which serves as the input of the trajectory prediction module.

C. Motion Prediction

Our trajectory prediction module is built upon MTR [10], a state-of-the-art model consisting of a scene context encoder and a motion decoder. We only provide a general introduction, and more details about the model can be found in [10].

For the i -th CAV, the scene context encoder extracts features from the agents' trajectories $\mathbf{X}_{t-T_h+1:t}$ and the local map information \mathbf{M}_t^i . The agents' trajectories are represented as polyline vectors [18], which are processed by a PointNet-like polyline encoder [34] to extract agent features. The map information is encoded by a Vision Transformer [35] to extract map features. Then, a Transformer encoder is used to capture the local scene context. Each layer uses multi-head attention with queries, keys, and values defined relative to previous layer outputs and position encodings, integrating the trajectory embeddings and map embeddings. Future agent movements are predicted via regression based on the extracted past agent features. These predictions are re-encoded by the same polyline encoder and merged with historical context features.

After obtaining the scene context features, a Transformer-based motion decoder is employed to generate multi-modal prediction hypotheses through joint optimization of global intention localization and local movement refinement. More specifically, K representative intention points $\mathbf{I} \in \mathbb{R}^{K \times 2}$ are generated by adopting the k -means clustering algorithm on the endpoints of ground truth trajectories ($K = 64$ in our setting), where each intention point represents an implicit motion mode that represents the motion direction. The local movement refinement enhances global intention localization by iteratively refining trajectories with fine-grained trajectory features. The dynamic searching query is initially set at the intention point, and updates dynamically based on the trajectory predicted at each decoder layer, serving as a spatial point's position embedding.

In the decoder, static intention queries transmit information across motion intentions while dynamic searching queries gather trajectory-specific information from the scene context. The updated motion query is expressed as $\mathbf{C}^j \in \mathbb{R}^{K \times D}$ in the j -th layer where D is the feature dimension. Each decoder layer adds a prediction head to \mathbf{C}^j for creating future trajectories. Due to the multi-modal nature of agents' behaviors, a Gaussian Mixture Model (GMM) is adopted for trajectory distributions. For each future time step $t' \in \{t+1, \dots, t+T_f\}$, we infer the likelihood p and parameters

$(\mu_x, \mu_y, \sigma_x, \sigma_y, \rho)$ of Gaussian components by

$$\mathbf{Z}_{t+1:t+T_f}^j = \text{MLP}(\mathbf{C}^j), \quad (1)$$

where $\mathbf{Z}_{t'}^j \in \mathbb{R}^{K \times 6}$ contains the parameters of K Gaussian components $\mathcal{N}_{1:K}(\mu_x, \sigma_x; \mu_y, \sigma_y; \rho)$ and the corresponding likelihoods $p_{1:K}$. The distribution of the agent's position at time t' is written as

$$P_{t'}^j(o) = \sum_{k=1}^K p_k \cdot \mathcal{N}_k(o_x - \mu_x, \sigma_x; o_y - \mu_y, \sigma_y; \rho), \quad (2)$$

where $P_{t'}^j(o)$ denotes the probability of the agent located at $o \in \mathbb{R}^2$ at time t' . The trajectory predictions of all the agents $\hat{\mathbf{X}}_{t+1:t+T_f}$ can be derived from the center points of corresponding Gaussian components.

D. Prediction Aggregation

Besides sharing the BEV features between CAVs, we also propose to transmit the prediction hypotheses generated by each CAV to others. Each CAV adopts an aggregation mechanism to fuse the predictions received from others with its own predictions. The underlying intuition is that the predictions for a certain agent obtained from different CAVs may have different levels of reliability. For example, a CAV closest to the predicted agent may generate better predictions than others. Thus, the predictions from different CAVs may complement each other, leading to the best final prediction.

More specifically, in a scenario with N_{CAV} CAVs and N_o predicted agents, the GMM prediction components for agent j by CAV i at time t are denoted as $\mathbf{Z}_{j,t+1:t+T_f}^i$. The local map and BEV features of CAV i are denoted as \mathbf{M}_t^i and \mathbf{H}_t^i , respectively. We aggregate the GMM components of the predicted trajectories, BEV features, and map information for all CAVs. For CAV i , it begins the aggregation process by concatenating its GMM, map, and BEV features:

$$\mathbf{E}_{j,t}^i = [\text{MLP}(f(\mathbf{Z}_{j,t+1:t+T_f}^i)), \text{MLP}(f(\mathbf{M}_t^i)), \text{MLP}(f(\mathbf{H}_t^i))], \quad (3)$$

Upon receiving the GMM components from other CAVs k ($1 \leq k \leq N_{\text{CAV}}, k \neq i$), the same map, BEV features from the ego are concatenated again:

$$\mathbf{E}_{j,t-1}^k = [\text{MLP}(f(\mathbf{Z}_{j,t:t+T_f-1}^k)), \text{MLP}(f(\mathbf{M}_t^i)), \text{MLP}(f(\mathbf{H}_t^i))], \quad (4)$$

followed by a multi-head self-attention to fuse the features across all CAVs,

$$\mathbf{G}_{j,t}^i = \text{MHA}([\mathbf{E}_{j,t}^i, \dots, \mathbf{E}_{j,t-1}^k]), 1 \leq k \leq N_{\text{CAV}}, k \neq i \quad (5)$$

where MHA is multi-head self-attention, f is the flatten operation, and $\mathbf{G}_{j,t}^i$ is the aggregated feature for agent j from the perspective of CAV i . The GMM components from other CAVs are delayed by one frame. Finally, two separate MLPs derive the aggregated Gaussian parameters by

$$\mathcal{N}_{j,1:K,t+1:t+T_f}^i(\mu_x, \sigma_x; \mu_y, \sigma_y; \rho) = \text{MLP}(\mathbf{G}_{j,t}^i), \quad (6)$$

$$p_{j,1:K,t+1:t+T_f}^i = \text{MLP}(\mathbf{G}_{j,t}^i), \quad (7)$$

which will be used to sample the final prediction hypotheses.

E. Loss Functions

Cooperative Object Detection. We adopt the same loss function as CoBEVT [5]. In particular, our framework incorporates the two convolutional layers for the detection head and employs the smooth $L1$ loss for bounding box localization $\mathcal{L}_{\text{det.loc}}$ and the focal loss for classification $\mathcal{L}_{\text{det.cls}}$, as outlined in [36]. The complete loss function is

$$\mathcal{L}_{\text{det}} = (\beta_{\text{loc}} \mathcal{L}_{\text{det.loc}} + \beta_{\text{cls}} \mathcal{L}_{\text{det.cls}}) / N_p, \quad (8)$$

where N_p denotes the count of positive instances, $\beta_{\text{loc}} = 2.0$, and $\beta_{\text{cls}} = 1.0$.

Motion Prediction. Our prediction model is trained with two loss terms. An $L1$ regression loss is used to refine the outputs in Eq. (1). We also employ a negative log-likelihood loss based on Eq. (2) to enhance the prediction accuracy of the actual trajectories. We take the weighted average of these two terms as the total loss, which is written as

$$\mathcal{L}_{\text{pred}} = \omega_{\text{loc}} \mathcal{L}_{\text{pred.loc}} + \omega_{\text{cls}} \mathcal{L}_{\text{pred.cls}}. \quad (9)$$

Following [21], we apply a hard-assignment technique for optimization by choosing the motion query pair that is closest to the ground truth (GT) trajectory's endpoint as the positive Gaussian component, determined by the distance between each intention point and the GT endpoint. The Gaussian regression loss is applied at every decoder layer, and the overall loss combines the auxiliary regression loss with the Gaussian regression losses with equal weights.

Prediction Aggregation. Our prediction aggregation module produces outputs in the same format as the motion prediction module, and we apply the same loss function as Eq. (9).

V. EXPERIMENTS

A. Dataset

We use the OPV2V dataset [4] to validate our approach. This dataset contains 73 traffic scenarios with a duration of about 25 seconds with multiple CAVs. A range of two to seven CAVs may appear concurrently, which are equipped with a LiDAR sensor and four cameras from different views. Following [5], we use a surrounding area of $100\text{m} \times 100\text{m}$ with a map resolution of 39 cm for evaluation. The dataset contains 6764, 1981, and 2719 frames for training, validation, and testing, respectively.

B. Evaluation Metrics

Cooperative Object Detection. We use the standard evaluation metrics as in [4], [37], including Average Precision (AP), Average Recall (AR), and F1-score at IoU thresholds of 0.3, 0.5 and 0.7, respectively.

Tracking. We use the standard evaluation metrics as in [32], including Multi-Object Tracking Accuracy (MOTA), Average Multi-Object Tracking Accuracy (AMOTA), Average Multi-Object Tracking Precision (AMOTP), scaled Average Multi-Object Tracking Accuracy (sAMOTA), Mostly Tracked Trajectories (MT), and Mostly Lost Trajectories (ML).

Motion Prediction. We predict the agents' trajectories for the future 5.0 seconds based on 1.0 seconds of historical observations. We use the standard evaluation metrics as in [10], including minADE₆ and minFDE₆.

TABLE I: The comparisons of cooperative object detection performance.

Communication Setting	Compression Ratio	AP 0.3↑	AR 0.3↑	F1 0.3↑	AP 0.5↑	AR 0.5↑	F1 0.5↑	AP 0.7↑	AR 0.7↑	F1 0.7↑	Bandwidth (M/s)↓
No Cooperation	N/A	0.76	0.39	0.52	0.75	0.39	0.51	0.61	0.35	0.45	N/A
No Delay	1x	0.94	0.47	0.63	0.93	0.47	0.63	0.88	0.46	0.60	80.0
No Delay	256x	0.93	0.47	0.63	0.93	0.47	0.63	0.88	0.46	0.60	0.31
Up to 100 ms Delay	1x	0.94	0.49	0.65	0.93	0.49	0.64	0.81	0.45	0.58	80.0
Up to 100 ms Delay	256x	0.93	0.47	0.63	0.92	0.47	0.62	0.82	0.44	0.58	0.31

TABLE II: The comparisons of multi-object tracking performance.

Communication Setting	Compression Ratio	sAMOTA ↑	AMOTA ↑	AMOTP ↑	MOTA ↑	MOTP ↑	MT ↑	ML ↓
No Cooperation	N/A	57.32	17.22	29.84	56.59	51.39	26.15	22.46
No Delay	1x	72.25	27.13	52.62	70.09	69.33	49.54	14.15
Up to 100 ms Delay	1x	67.17	23.60	46.35	65.63	64.99	40.92	14.46
Up to 100 ms Delay	256x	66.99	23.60	45.83	66.98	64.33	42.77	14.46

TABLE III: The comparisons of motion prediction performance (meter).

Cooperation Type	minADE ₆ @1s ↓	minADE ₆ @3s ↓	minADE ₆ @5s ↓	minFDE ₆ @1s ↓	minFDE ₆ @3s ↓	minFDE ₆ @5s ↓
No Cooperation	0.3817	1.1082	2.1095	0.6558	2.3503	5.0242
Cooperative Perception Only	0.3398	0.9567	1.8556	0.5513	2.0008	4.3054
Cooperative Prediction (Ours)	0.3252	0.8977	1.7472	0.5199	1.8306	4.0531

C. Implementation Details

Cooperative Object Detection. CoBEVT [5] assumes no delay in the communication between CAVs, which may not be realistic due to hardware or wireless communication constraints. To address this limitation, our model allows for up to a 100 ms (i.e., 1 frame) delay in receiving the messages (i.e., BEV features) from other CAVs. In addition, our BEV features are compressed by 256 times compared with that in CoBEVT. Instead of selecting a single CAV as the ego vehicle in the original OPV2V traffic scenarios as in [5], we augment the training data samples by treating each of the CAVs in the scene as the ego vehicle. We train our model using the AdamW [38] optimizer with a learning rate scheduler starting at 1×10^{-3} and reduced every 10 epochs.

Tracking. In our setting, we set $F_{\min} = 3$ and $\text{Age}_{\min} = 2$ in the birth/death memory module. The data association module uses a threshold of $\text{IoU}_{\min} = 0.01$ for vehicles, and Dist_{\max} is set to 10. More details can be found in [32].

Motion Prediction. We use 6 encoder layers for context encoding with a hidden feature dimension of 256. The decoder employs 6 layers and 64 motion query pairs, determined by k -means clustering on the training set. We pre-train the prediction model with an AdamW optimizer [38] with a learning rate of 1×10^{-4} and a batch size of 80 over 30 epochs. More details can be found in [10].

Prediction Aggregation. We use three MLPs to encode the GMM parameters, map features, and BEV features, respectively. Then, an 8-head, 5-layer transformer encoder is used to aggregate the features, followed by two MLPs to decode the outputs into the final GMM trajectory and scores, which follow the same format as the outputs of the prediction module. We train the aggregation module with a learning rate of 1×10^{-4} and fine-tune the prediction module with a reduced learning rate of 1×10^{-6} . The learning rates decay in the same manner as the prediction model. We train the

model for 30 epochs with a batch size of 8.

D. Quantitative and Ablative Results

Cooperative Object Detection. In Table I, we demonstrate the effects of multi-vehicle cooperation, communication delay, and compression ratio of BEV features on the object detection performance. The comparisons between *No Cooperation* and other settings show the improvement brought by the CAV communications. To mimic the real-world constraints, we introduce a 100 ms communication delay, substantially shorter than typical human reaction times to visual stimuli, yet realistic within current wireless communication capabilities. We notice the performance decreases slightly at an IOU threshold of 0.7 and remains comparable in other settings, which can be attributed to the temporal misalignment of shared data. In addition, a compression ratio of 256 only slightly degrades system performance but significantly reduces the bandwidth requirements, demonstrating efficiency in data transmission when sharing BEV features from one CAV to another. Based on these findings, we adopt a 256x compression ratio for BEV features and accommodate a 100 ms communication latency between CAVs, which balances between the model performance and hardware constraints (i.e., bandwidth, latency).

Tracking. We show the enhancement of tracking performance enabled by multi-vehicle cooperations in Table II. V2V communication enables the fusion of information across different CAVs, which significantly increases the number of true positives (i.e., accurately detected objects) and reduces the instances of false positives and false negatives (i.e., missing objects). The improvement in object detection is a major cause for the enhanced performance of the tracking system. Furthermore, despite the substantial BEV feature compression, we observe no detrimental effect on the tracking performance, which implies that tracking remains robust even under significant feature compression.

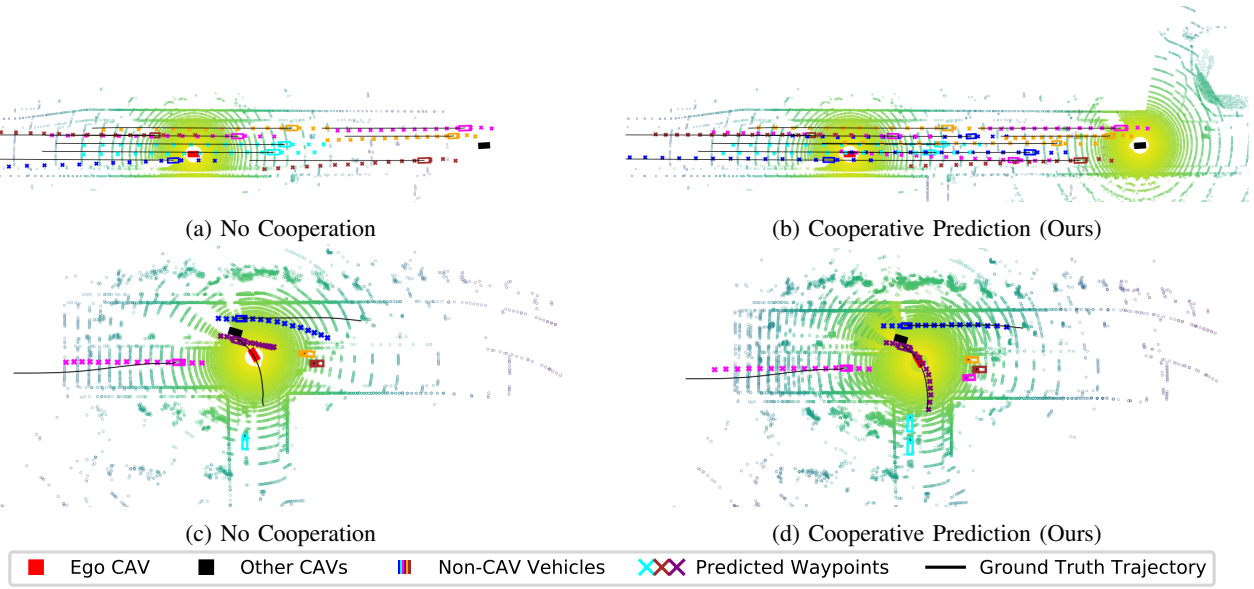


Fig. 3: The visualizations of predicted trajectories under different model settings.

Cooperative Motion Prediction. We present a series of quantitative and ablation studies on cooperative motion prediction. The detailed results are shown in Table III and Fig. 4. The *Cooperative Perception Only* setting does not include our prediction aggregation module, and CAVs only share the compressed BEV features in the perception stage. Table III shows that cooperative perception enhances the prediction performance by a large margin and the improvement becomes larger as the prediction horizon increases. At 5s, our model achieved a 12.3%/17.2% reduction in minADE_6 compared with the *Cooperative Perception Only* and *No Cooperation* settings, respectively. The reason is that cooperative perception improves the detection accuracy and thus the quality of historical trajectories employed by the prediction module. Moreover, the prediction aggregation module allows CAVs to leverage the predictions from others to collectively compensate for their prediction in challenging and ambiguous situations. In Fig. 4, our cooperation modules bring more benefits as the CAVs in the scene cover larger fields of view. Specifically, we approximate the perception coverage area from the CAVs as the area of the convex hull formed by the CAVs. As this area grows to over 200m^2 , the performance improvement of our model climbs to 17.5%/28.4%, compared to the other two settings. The reason is that the communication between CAVs enhances the situational awareness of the ego vehicle with more comprehensive, precise detections of surrounding objects and richer insights for future prediction from various perspectives.

E. Qualitative Results

We provide the visualizations of the predicted vehicle trajectories in two distinct scenarios in Fig. 3 to illustrate the effectiveness of cooperative prediction. Fig. 3(a) and 3(b) depict the same scenario involving two CAVs. It is evident that cooperative prediction significantly reduces the number of non-CAV vehicles that are overlooked, which highlights the enhanced sensing capability brought by cooperations,

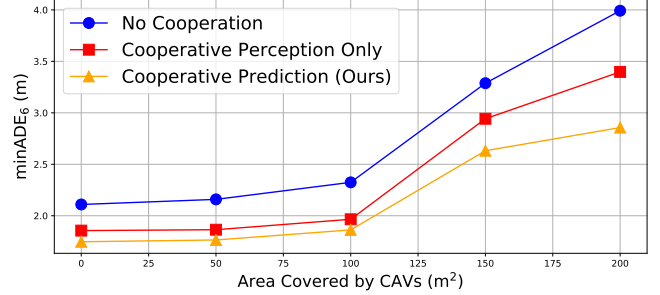


Fig. 4: A comparison of motion prediction performance under different areas covered by CAVs. The area is calculated based on the smallest convex hull that covers all the CAVs.

allowing each CAV to extend its perception range and detect vehicles that might otherwise be missed. Fig. 3(c) and 3(d) show another scenario, demonstrating the improved accuracy of cooperative prediction. In this case, the predicted trajectories by cooperative prediction align more closely with the ground truth thanks to information sharing between CAVs.

VI. CONCLUSION

In this paper, we introduce the first-of-its-kind cooperative motion prediction framework that advances the cooperative capabilities of CAVs, addressing the crucial need for safe and robust decision making in dynamic environments. By integrating cooperative perception with trajectory prediction, our work marks a pioneering effort in the realm of connected and automated vehicles, which enables CAVs to share and fuse data from LiDAR point clouds to improve object detection, tracking, and motion prediction. Specifically, our contributions include a latency-robust cooperative prediction pipeline, communication bandwidth analysis, and a cooperative aggregation mechanism for motion prediction, which advance CAV performance and set a benchmark for future research. Our pipeline does not yield a fully end-to-end approach due to the non-differentiable tracker. Future

work will focus on developing a fully differentiable pipeline with more advanced architectures for a seamless cooperative system. We will also investigate multi-modal sensor fusion with heterogeneous CAVs to improve flexibility.

REFERENCES

- [1] H. Qiu, F. Ahmad, F. Bai, M. Gruteser, and R. Govindan, "Avr: Augmented vehicular reality," in *Proceedings of the 16th Annual International Conference on Mobile Systems, Applications, and Services (MobiSys)*, ser. MobiSys '18, Munich, Germany: ACM, Jan. 1, 2018, pp. 81–95, published.
- [2] H. Qiu, P. Huang, N. Asavisanu, X. Liu, K. Psounis, and R. Govindan, "Autocast: Scalable infrastructure-less cooperative perception for distributed collaborative driving," in *Proceedings of the 20th Annual International Conference on Mobile Systems, Applications, and Services*, 2022.
- [3] T. Wang, S. Manivasagam, M. Liang, B. Yang, W. Zeng, and R. Urtasun, "V2vnet: Vehicle-to-vehicle communication for joint perception and prediction," in *European Conference on Computer Vision*, Springer, 2020, pp. 605–621.
- [4] R. Xu, H. Xiang, X. Xia, X. Han, J. Li, and J. Ma, "Opv2v: An open benchmark dataset and fusion pipeline for perception with vehicle-to-vehicle communication," in *International Conference on Robotics and Automation (ICRA)*, 2022.
- [5] R. Xu, Z. Tu, H. Xiang, W. Shao, B. Zhou, and J. Ma, "Cobevt: Cooperative bird's eye view semantic segmentation with sparse transformers," in *Conference on Robot Learning*, 2022, pp. 989–1000.
- [6] R. Xu, H. Xiang, Z. Tu, X. Xia, M. Yang, and J. Ma, "V2xvit: Vehicle-to-everything cooperative perception with vision transformer," in *European Conference on Computer Vision*, Springer, 2022, pp. 107–124.
- [7] Y. Hu, S. Chen, Y. Zhang, and X. Gu, "Collaborative motion prediction via neural motion message passing," in *IEEE/CVF Conference on Computer Vision and Pattern Recognition*, 2020, pp. 6318–6327.
- [8] D. Choi, J. Yim, M. Baek, and S. Lee, "Machine learning-based vehicle trajectory prediction using v2v communications and on-board sensors," *Electronics*, vol. 10, p. 420, Feb. 2021.
- [9] H. Guo, L.-l. Rui, and Z.-p. Gao, "V2v task offloading algorithm with lstm-based spatiotemporal trajectory prediction model in svcns," *IEEE Transactions on Vehicular Technology*, vol. 71, no. 10, pp. 11 017–11 032, 2022.
- [10] S. Shi, L. Jiang, D. Dai, and B. Schiele, "Motion transformer with global intention localization and local movement refinement," in *Advances in Neural Information Processing Systems*, 2022.
- [11] S. Shi, L. Jiang, D. Dai, and B. Schiele, "Mtr++: Multi-agent motion prediction with symmetric scene modeling and guided intention querying," *IEEE Transactions on Pattern Analysis and Machine Intelligence*, 2024.
- [12] Y. Wang and J. Chen, "Eqdrive: Efficient equivariant motion forecasting with multi-modality for autonomous driving," *arXiv preprint arXiv:2310.17540*, 2023.
- [13] Z. Y. Rawashdeh and Z. Wang, "Collaborative automated driving: A machine learning-based method to enhance the accuracy of shared information," in *International Conference on Intelligent Transportation Systems (ITSC)*, 2018, pp. 3961–3966.
- [14] H. Qiu*, J. Cui*, D. Chen, P. Stone, and Y. Zhu, "Coopernaut: End-to-end driving with cooperative perception for networked vehicles," in *Proceedings of the IEEE/CVF Conference on Computer Vision and Pattern Recognition*, 2022.
- [15] D. Qiao and F. H. Zulkernine, "Adaptive feature fusion for cooperative perception using lidar point clouds," in *IEEE/CVF Winter Conference on Applications of Computer Vision*, IEEE, 2023, pp. 1186–1195.
- [16] H. Xiang, R. Xu, and J. Ma, "Hm-vit: Hetero-modal vehicle-to-vehicle cooperative perception with vision transformer," in *IEEE/CVF International Conference on Computer Vision*, IEEE, 2023, pp. 284–295.
- [17] J. Li, F. Yang, M. Tomizuka, and C. Choi, "Evolvegaph: Multi-agent trajectory prediction with dynamic relational reasoning," in *Advances in Neural Information Processing Systems*, 2020.
- [18] J. Gao, C. Sun, H. Zhao, *et al.*, "Vectornet: Encoding HD maps and agent dynamics from vectorized representation," in *IEEE/CVF Conference on Computer Vision and Pattern Recognition*, 2020, pp. 11 522–11 530.
- [19] M. Toyungyernsub, E. Yel, J. Li, and M. J. Kochenderfer, "Dynamics-aware spatiotemporal occupancy prediction in urban environments," in *2022 IEEE/RSJ International Conference on Intelligent Robots and Systems (IROS)*, IEEE, 2022, pp. 10 836–10 841.
- [20] J. Li, H. Ma, Z. Zhang, J. Li, and M. Tomizuka, "Spatio-temporal graph dual-attention network for multi-agent prediction and tracking," *IEEE Transactions on Intelligent Transportation Systems*, vol. 23, no. 8, pp. 10 556–10 569, 2021.
- [21] B. Varadarajan, A. Hefny, A. Srivastava, *et al.*, "Multipath++: Efficient information fusion and trajectory aggregation for behavior prediction," in *International Conference on Robotics and Automation (ICRA)*, 2022.
- [22] H. Girase, H. Gang, S. Malla, *et al.*, "Loki: Long term and key intentions for trajectory prediction," in *Proceedings of the IEEE/CVF International Conference on Computer Vision*, 2021, pp. 9803–9812.
- [23] C. Choi, J. H. Choi, J. Li, and S. Malla, "Shared cross-modal trajectory prediction for autonomous driving," in *Proceedings of the IEEE/CVF Conference on Computer Vision and Pattern Recognition*, 2021, pp. 244–253.
- [24] Q. Sun, X. Huang, J. Gu, B. C. Williams, and H. Zhao, "M2I: from factored marginal trajectory prediction to interactive prediction," in *IEEE/CVF Conference on Computer Vision and Pattern Recognition*, IEEE, 2022, pp. 6533–6542.
- [25] B. Lange, J. Li, and M. J. Kochenderfer, "Scene informer: Anchor-based occlusion inference and trajectory prediction in partially observable environments," in *International Conference on Robotics and Automation (ICRA)*, 2024.
- [26] V. M. Dax, J. Li, E. Sachdeva, N. Agarwal, and M. J. Kochenderfer, "Disentangled neural relational inference for interpretable motion prediction," *IEEE Robotics and Automation Letters*, 2023.
- [27] H. Ruan, H. Yu, W. Yang, S. Fan, Y. Tang, and Z. Nie, "Learning cooperative trajectory representations for motion forecasting," *arXiv preprint arXiv:2311.00371*, 2023.
- [28] K. Li, Y. Chen, M. Shan, J. Li, S. Worrall, and E. Nebot, "Game theory-based simultaneous prediction and planning for autonomous vehicle navigation in crowded environments," in *2023 IEEE 26th International Conference on Intelligent Transportation Systems (ITSC)*, IEEE, 2023, pp. 2977–2984.
- [29] Y. Wang and J. Chen, "Equivariant map and agent geometry for autonomous driving motion prediction," in *2023 International Conference on Electrical, Computer and Energy Technologies (ICECET)*, IEEE, 2023, pp. 1–6.
- [30] J. Gu, C. Sun, and H. Zhao, "Densetnt: End-to-end trajectory prediction from dense goal sets," in *IEEE/CVF International Conference on Computer Vision*, IEEE, 2021, pp. 15 283–15 292.
- [31] J. Ngiam, V. Vasudevan, B. Caine, *et al.*, "Scene transformer: A unified architecture for predicting future trajectories of multiple agents," in *International Conference on Learning Representations*, 2022.
- [32] X. Weng, J. Wang, D. Held, and K. Kitani, "3d multi-object tracking: A baseline and new evaluation metrics," in *IEEE/RSJ International Conference on Intelligent Robots and Systems*, IEEE, 2020, pp. 10 359–10 366.
- [33] A. H. Lang, S. Vora, H. Caesar, L. Zhou, J. Yang, and O. Beijbom, "Pointpillars: Fast encoders for object detection from point clouds," in *IEEE/CVF Conference on Computer Vision and Pattern Recognition*, 2019.
- [34] R. Q. Charles, H. Su, M. Kaichun, and L. J. Guibas, "Pointnet: Deep learning on point sets for 3d classification and segmentation," in *2017 IEEE Conference on Computer Vision and Pattern Recognition (CVPR)*, 2017.
- [35] A. Dosovitskiy, L. Beyer, A. Kolesnikov, *et al.*, "An image is worth 16x16 words: Transformers for image recognition at scale," in *International Conference on Learning Representations*, 2020.
- [36] T.-Y. Lin, P. Goyal, R. Girshick, K. He, and P. Dollár, "Focal loss for dense object detection," in *IEEE International Conference on Computer Vision (ICCV)*, 2017.
- [37] R. Xu, W. Chen, H. Xiang, X. Xia, L. Liu, and J. Ma, "Model-agnostic multi-agent perception framework," in *IEEE International Conference on Robotics and Automation*, IEEE, 2023, pp. 1471–1478.
- [38] I. Loshchilov and F. Hutter, "Decoupled weight decay regularization," in *International Conference on Learning Representations*, 2018.